Link to publication

The final published article is available from http://jcs.biologists.org

University of Bath

Stimulus-induced uncoupling of extracellular signal-regulated kinase phosphorylation from nuclear localization is dependent on docking domain interactions

Christopher J. Caunt[1] and Craig A. McArdle[2]

[1]Dept. of Biology and Biochemistry, University of Bath, Claverton Down, Bath, BA2 7AY, UK. [2]Laboratories for Integrative Neuroscience and Endocrinology, Dept. of Clinical Sciences at South Bristol, University of Bristol, Whitson Street, Bristol, BS1 3NY, UK.

Abstract

Many stimuli activate the extracellular signal regulated kinase (ERK) by phosphorylation on the TEY motif. Activated ERK characteristically accumulates in the nucleus, but mechanisms involved are unclear. Using automated microscopy to explore ERK regulation in single intact cells, we find that when protein kinase C or epidermal growth factor receptors are activated, a substantial fraction of the ERK nuclear localization response is uncoupled from TEY phosphorylation. This phosphorylation unattributable nuclear localization response occurs in the presence of tyrosine phosphatase and protein synthesis inhibitors. It was also seen with a catalytically inactive ERK2-GFP mutant, and with a mutant incapable of binding the DEF (docking site for ERK, F/Y-X-F/Y-P) domains found in many ERK binding partners. It was, however, reduced by MEK inhibition and by mutations preventing either TEY phosphorylation or D (docking)-domain dependent ERK binding (D319N). Thus, we show that MEK catalysed ERK phosphorylation is necessary but not sufficient for the full nuclear localization response: there is an additional phosphorylation unattributable component of the response that does not reflect induced expression of nuclear anchors and is independent of ERK catalytic activity or DEF-domain binding. It is, however, dependent upon D-domain binding, highlighting distinct roles of ERK motifs during nuclear targeting.

Introduction

A wide variety of extracellular signals activate the Raf-MEK-ERK pathway. In this cascade, Raf isoforms are recruited to the cell membrane for activation, which phosphorylate and activate MEK (MAPK/ERK kinase). Activated MEK in turn phosphorylates ERK1 and 2 (referred to as ERK herein) on Thr and Tyr residues of a TEY activation loop (Caunt et al., 2006a; Raman et al., 2007). ERK is chiefly cytoplasmic in resting cells, but activation causes its accumulation in the nucleus (Chen et al., 1992; Lenormand et al., 1993; Lidke et al., 2010). This is crucial for ERK to access transcriptional targets, and correct localization is essential for the integrity of cell fate decisions, such as proliferation and differentiation (Brunet et al., 1999; Robinson et al., 1998). ERK does not contain intrinsic nuclear localization or export signals, and relies on dynamic association with a wide repertoire of proteins for appropriate subcellular targeting (von Kriegsheim et al., 2009). The distribution of ERK between the nucleus and the cytoplasm is dependent upon rates of nuclear entry and exit (Costa et al. 2006; Lidke et al. 2010). ERK can enter and exit the nucleus via an energy-independent process that is facilitated by direct interaction with nuclear pore proteins and TEY phosphorylated ERK can also be imported by a second process requiring both energy and cytosolic factors (Ranganathan et al. 2006; Yazicioglu et al. 2007; Whitehurst et al. 2002). Cytoplasmic and nuclear binding proteins can also influence ERK distribution by affecting the fraction of ERK available for movement to or from the nucleus. MEK is a major cytoplasmic scaffold of ERK and MEK-directed ERK phosphorylation of the TEY motif causes its liberation from MEK, facilitating its interaction with other proteins including those of the nuclear pore complex. In this way, MEK activation characteristically increases the nuclear localisation of ERK, an effect that is dependent upon the TEY motif (Adachi et al., 1999; Chuderland et al., 2008b; Fukuda et al., 1997; Lenormand et al., 1998; Wolf et al., 2001) but not on ERK catalytic activity (Adachi et al., 1999; Gonzalez et al., 1993; Khokhlatchev et al., 1998; Yazicioglu et al., 2007). Other proteins that that can cause cytoplasmic retention of ERK include PEA-15, dual specificity phosphatase (DUSP) 6, β-arrestin and Sef (Brunet et al., 1999; Caunt et al., 2006b; Formstecher et al. 2001; Karlsson et al., 2004; Luttrell et al., 2001; Tohgo et al., 2002; Torii et al., 2004). In contrast, expression of nuclear DUSPs 2, 4 and 5 can mediate dephosphorylation and nuclear anchoring of ERK in sustained phases of signaling (Caunt et al., 2008a;

Caunt et al., 2008b; Mandl et al., 2005; Volmat et al., 2001). Thus, many proteins influence ERK compartmentalization, and correct interpretation of these often conflicting signals is essential during dynamic changes in localization.

The specificity of the association of ERK with its binding proteins is dictated by docking domains. The ERK common docking (CD) motif is distal to the catalytic site and binds to Lys and Arg-rich sequences, known as D (docking)-domains (Tanoue et al., 2001). Another key docking site in ERK protein partners is termed the DEF (docking site for ERK, F/Y-X-F/Y-P) motif, which binds to a DEF-binding pocket (DBP) adjacent to the catalytic site of ERK (Jacobs et al., 1999; Lee et al., 2004). ERK protein partners can contain either or both D- and DEF-domains allowing intricate regulation of ERK recognition (Dimitri et al., 2005; Jacobs et al., 1999; Shin et al., 2010). The MEK-ERK interaction is multivalent, involving both the CD motif and the DBP of ERK (Robinson et al., 2002). Phosphorylation and release of ERK from MEK therefore exposes these docking sites during stimulus-mediated responses. Recent studies have shown that D319N and Y261A mutations can interfere with ERK binding to partner D- or DEF-domain containing proteins, respectively, in intact cells without affecting phosphorylation or overall catalytic activation by MEK (Caunt et al., 2008a; Caunt et al., 2008b; Dimitri et al., 2005; Shin et al., 2010). These mutations can therefore be used to identify ERK responses that are dependent on D- or DEF-domain interactions.

Uncoupling of ERK phosphorylation and nuclear localization responses occurs in a number of models, but the mechanisms remain largely unknown. Most previous work exploring relationships between ERK phosphorylation and compartmentalization in attached cells has involved biochemical assays with cell homogenates or microscopy with relatively small cell numbers. Here, we have taken a novel approach, using automated fluorescence microscopy and image analysis to monitor ppERK1/2 levels and the nuclear:cytoplasmic (N:C) ERK1/2 ratio in large numbers of single attached cells. This enables response characteristics to be defined from frequency distributions and in cell sub-populations selected (i.e. binned) according to ppERK1/2 level. Using population averaged data we found that protein kinase C (PKC) activation using phorbol 12, 13 dibutyrate (PDBu) and epidermal growth factor (EGF) caused the expected dose- and time-

dependent increases in ppERK1/2 and ERK1/2 N:C. However, with data binned according to ppERK1/2 levels, both activators still caused a pronounced increase in ERK1/2 N:C. This reveals a clear component of the endogenous ERK nuclear localization response that cannot be attributed to TEY phosphorylation of ERK. Exploring mechanisms (with chemical inhibitors and a system in which endogenous ERK is replaced with wild-type or mutated ERK2-GFP) revealed that this component of the response was dependent on MEK activity and TEY phosphorylation of ERK. It was also dependent upon D-domain dependent binding but not on DEF-domain dependent binding, protein neosynthesis or ERK catalytic activity. Thus, we have found that MEK-directed TEY phosphorylation of ERK is necessary but not sufficient for the full PDBu- and EGF-stimulated nuclear localization response. There is an additional TEY phosphorylation unattributable component of the response that is dependent upon D-domain mediated binding of ERK to, as yet, unidentified partners.

Results

Using high-content microscopy to study ERK phosphorylation and localization

We examined spatial and temporal aspects of ERK regulation by immunofluorescence microscopy. Total ERK1/2 and ppERK1/2 were stained simultaneously and quantified using a high-content image platform for automated image acquisition and analysis. Stimulation of conventional and atypical PKC isoforms with PDBu caused dose and time-dependent increases in whole cell levels of dual phosphorylated ERK (ppERK1/2), providing a measure for ERK activation. It also caused dose- and time-dependent increases in the nuclear:cytoplasmic (N:C) ERK1/2 ratio, providing a measure for nuclear localization. The kinetics of these two responses differed (Fig. 1). The effect of PDBu on ppERK1/2 levels was maximal at 5 minutes and then decreased to a plateau level (10-30% of maximal) that was maintained from 60 minutes to 6 hours. This is consistent with earlier data (Caunt et al., 2008a; Caunt et al., 2008b) and with response kinetics obtained by Western blotting for ppERK1/2 in whole cell lysates (Fig. 1). Western blotting revealed sustained MEK phosphorylation from 5-240 minutes so the reduction in ppERK1/2 levels occurred in spite of ongoing MEK activation over this period. The ERK nuclear localization response also increased to a peak at 5 minutes then reduced briefly before increasing again to a maximum at 2 hours (1 µM PDBu) or 6 hours (0.1 µM PDBu). This uncoupling of the relatively transient effect of PDBu on ppERK1/2 from its more sustained effect on ERK1/2 N:C has previously been attributed to

nuclear DUSPs that can both dephosphorylate and anchor ERK in the nucleus (Caunt et al., 2008a; Caunt et al., 2008b; Mandl et al., 2005; Volmat et al., 2001). Consistent with this, we found that PDBu also caused a pronounced increase in whole cell levels of DUSP1 (the prototypic nuclear DUSP) at 1–4 hours after stimulation (Fig. 1).

Analysis of cell sub-populations reveals uncoupling of ERK phosphorylation from nuclear localization.

The data described above were derived from population averages (thousands of imaged or lysed cells) but the microscopy methods used also provide data on each individual cell. This is particularly important for ERK signaling because at the single cell level stimuli cause digital "all-or-nothing" responses in some models and graded responses in others (Ferrell and Machleder, 1998; Lin et al., 2009; Mackeigan et al., 2005; Whitehurst et al., 2004). Moreover, a recent study found that graded ERK phosphorylation causes digital increases in immediate early gene expression, raising the question of whether ERK translocation to the nucleus is digital or graded (Mackeigan et al., 2005). To assess this, we generated frequency distribution histograms for whole cell ppERK1/2 levels and ERK1/2 N:C ratios in control and PDBu stimulated cells (Fig. 2A). As expected, stimulation for 5 minutes with 1 µM PDBu shifted the frequency-response plots rightward, yielding near-normal distribution curves for both measures with ppERK1/2 and ERK1/2 N:C mode values increased approx. 8 and 2-fold above controls (respectively). The histograms obtained with 0.1 µM PDBu were also near normally distributed with intermediate mode values (6 and 1.6 fold above control for ppERK1/2 and ERK1/2 N:C, respectively). This is in sharp contrast to the bimodal distribution seen with digital responses (Lin et al., 2009), revealing that ERK1/2 phosphorylation and nuclear localization are both graded responses in HeLa cells. Similar data were seen in MCF7 cells (not shown).

A further feature of these plots is that whole cell ppERK1/2 values were broadly spread (99% of cells within a 30-fold range of ppERK1/2 levels) as compared to the much tighter N:C ERK1/2 range (99% of cells within 3-fold N:C ERK1/2 range) (Fig. 2A). This suggests uncoupling of the responses, with relatively constant nuclear localization over a broad range of ppERK1/2 levels. To test for this, we sorted the cells into bins according to ppERK1/2 level (each spanning 80 arbitrary fluorescence units (AFU)) and for each bin, plotted the mean ppERK1/2 value against the mean ERK1/2 N:C ratio in the same cells. In control cells this revealed a positive correlation between the ppERK1/2 and N:C

ERK1/2 measures (Fig. 2B). In contrast, when cells were treated for 2 hours with 1 µM PDBu an entirely different relationship was observed with the N:C ERK1/2 ratio decreasing with increased ppERK1/2 levels but remaining greater than that of control cells in all ppERK1/2 bins (Fig.2B). This uncoupling of the two responses most likely reflects the ability of PDBu to increase expression of nuclear DUSPs that dephosphorylate and scaffold ERK in the nucleus (Caunt et al., 2008a; Caunt et al., 2008b; Mandl et al., 2005; Volmat et al., 2001). Surprisingly however, 5 minutes stimulation with PDBu also caused a substantial increase in ERK1/2 N:C ratio over a wide range of ppERK1/2 bins in spite of the fact that this is insufficient time for increased DUSP expression (Fig. 2B). Similar data were obtained in MCF7 cells and in primary mouse embryonal fibroblast cultures. In all three cell types data binning revealed a pronounced uncoupling of the ppERK1/2 response from the ERK1/2 N:C response after 2 hours of stimulation with 1 µM PDBu, and a less pronounced but statistically significant uncoupling at 5 minutes (Fig. 2 and Supplemental Fig. 2).

The data outlined above demonstrate that the effects of PDBu on ERK nuclear distribution cannot solely be attributed to TEY phosphorylation, because PDBu causes pronounced increases in ERK1/2 N:C in the absence of any measurable increase in ppERK1/2 (i.e. using bins with matched and indistinguishable ppERK1/2 levels). They also reveal that analysis of the subset of cells within a relatively narrow ppERK1/2 range provides a simple means of quantifying this component in isolation. We next stimulated cells for 5 minutes with varied concentrations of PDBu and compared population average responses with those in cell subsets matched for ppERK1/2 levels. With population averaged data, PDBu caused the expected concentration-dependent increases in ppERK1/2 and N:C ERK1/2 ratio with comparable potency for both effects (log EC_{50} values -6.9±0.2 and -7.2±0.2 respectively, Fig. 3). When similar plots were generated only for cells within a narrow range of ppERK1/2 levels (240-280 AFU), PDBu caused no measurable increase in ppERK1/2 but did cause a concentration-dependent increase in N:C ERK1/2 ratio. These data reveal that PDBu-mediated nuclear localization of ERK1/2 is proportional to stimulus, even under conditions where it is not proportional to ppERK1/2 level. Thus, we show for the first time the extent to which mechanisms other than phosphorylation-dependent release from MEK are employed to achieve the full ERK nuclear localization response elicited by PKC activation.

We also determined the time-course of PDBu action by stimulating cells with 1 µM PDBu for 5 minutes - 6 hours and generated single cell frequency distribution plots (for ppERK1/2 and ERK1/2 N:C) and found as expected, that the mode values for ppERK1/2 and ERK1/2 N:C paralleled the population average responses (Supplemental Fig.1 and Fig. 4A). We also binned the data according to ppERK1/2 level and plotted this against ERK1/2 N:C (as above) and this revealed clear uncoupling of the responses at all time points (Supplemental Fig. 1). This can readily be visualized by plotting the time-course of the PDBu effect using only cells within a single relatively low ppERK1/2 bin (240-320 AFU). As shown (Fig. 4) PDBu caused a pronounced increase in N:C ERK1/2 ratio in this sub-population in spite of the fact that it caused no measurable increase in ppERK1/2. The time-courses of effects on ERK1/2 distribution were very similar in the binned and population averaged responses although the transient increase in ppERK1/2 levels was clearly seen in the population average data (compare Fig. 4A and 4B).

We next used the same approach to explore stimulus-specificity. Population averaged data revealed that epidermal growth factor (EGF) causes a transient increase in ppERK1/2 and also increases the N:C ERK1/2 ratio. As in earlier work (Caunt et al., 2008a; Caunt et al., 2008b; Whitehurst et al., 2004) the magnitude and kinetics of the EGF effect on ppERK1/2 levels were similar to those seen with PDBu, but EGF was less effective than PDBu at driving ERK1/2 nuclear localization (Fig. 5A). The tyrosine phosphatase inhibitor sodium orthovanadate (vanadate) caused a slow and near linear increase in ppERK1/2 (without any increase in N:C ERK1/2 ratio) demonstrating involvement of tyrosine phosphatases in basal ppERK1/2 turnover (Fig. 5A). We also binned the single cell data according to ppERK1/2 level in order to compare effects of these stimuli under conditions with comparable average ppERK1/2 levels (5 minutes stimulation for PDBu and EGF, and 6 hours for vanadate). This revealed the expected positive correlation between ppERK1/2 levels and N:C ERK1/2 ratio in control cells and clear uncoupling of the responses, with PDBu increasing N:C ERK1/2 as compared to control cells matched for ppERK1/2. Similar uncoupling was seen in EGF-stimulated cells, but not in response to vanadate, where only a modest elevation in ERK1/2 N:C occurred, even at very high ppERK1/2 levels (Fig. 5B). These data echo earlier results showing that ERK nuclear accumulation is dictated by stimulus type (Whitehurst et al., 2004), and support the idea that stimulus-induced and basal trafficking

of ERK operate via distinct mechanisms (Casar et al., 2007).

PDBu-induced uncoupling of ERK phosphorylation from nuclear localization is dependent on MEK.
We next used a range of pharmacological inhibitors to explore possible mechanisms underlying ERK activation and nuclear localization. Using maximally effective inhibitor concentrations established in control assays (not shown), we treated HeLa cells for 10 minutes prior to acute (5 minute) stimulation with PDBu. Population averaged data revealed that the effects of PDBu on ppERK1/2 and N:C ERK1/2 ratio were dependent upon PKC and MEK (inhibited by Ro31-8425 and PD184352) and independent of Src (uninfluenced by SU6656). The responses were also unaltered by vanadate or cycloheximide (CHX), demonstrating that tyrosine phosphatases and protein neosynthesis do not influence these acute responses (although they do alter responses to long-term PDBu stimulation in this model; unpublished data and (Caunt et al., 2008a; Caunt et al., 2008b)). Focusing on cell sub-sets with a narrow range of ppERK1/2 levels (240-320 AFU) again revealed a dose-dependent effect of PDBu on ERK1/2 N:C (Fig. 6B). This nuclear localization response was completely blocked by Ro31-8425 and PD184352, demonstrating dependence on PKC and MEK, respectively. However, it was uninfluenced by SU6656, vanadate and CHX, demonstrating independence from Src, tyrosine phosphatase activity and protein neosynthesis. These effects were seen under conditions matched for low ppERK1/2 levels and in which ppERK1/2 was not measurably altered by the stimulus or the inhibitors (Fig. 6B, lower right panel). Thus the component of the acute PDBu-induced translocation response that cannot be solely attributed to TEY phosphorylation of ERK1/2 is nevertheless dependent on MEK activation. This may explain why this component is seen with stimuli that activate MEK (PDBu and EGF) but not with a treatment that increases ppERK1/2 by phosphatase inhibition (vanadate) (Fig. 5B).

PDBu-induced uncoupling of ERK phosphorylation from translocation is dependent on D-domains.
To further explore relationships between ERK phosphorylation and localization we used a previously characterised system in which siRNAs are used to reduce expression of endogenous ERK, and recombinant adenoviruses (Ad) are used to introduce GFP-tagged wild-type (WT) or mutated ERK2 reporters. As shown (Fig. 7A) the siRNAs reduced endogenous ERK levels by >95%. This was paralleled by reduced PDBu-stimulated ERK phosphorylation (as measured by cell imaging or by Western blotting) and Egr-1 Luc activity (early

growth response-1 promoter-luciferase reporter, used as a transcriptional readout for ERK activation). Addition of Ad ERK2-GFP restored ERK2 expression levels, as well as PDBu-stimulated ERK2 phosphorylation and Egr-1 Luc responses to wild-type levels (Fig. 7A, data not shown and (Caunt et al., 2008a; Caunt et al., 2008b)). A similar approach was used to add-back mutated ERK2-GFP constructs (after siRNA knock-down) and Western blotting revealed comparable expression levels for WT ERK2-GFP and for reporters containing K52R (catalytically inactive), T183/Y185A (non-TEY phosphorylatable), Y261A (deficient in binding DEF domains) and D319N (deficient in binding D-domains) variants of ERK2-GFP. None of the mutations inhibited MEK expression or PDBu-stimulated MEK phosphorylation (Fig. 7A).

Imaging assays (population averaged data) were then used to define effects of these mutations on responses to PDBu. As shown (Fig. 7B), 5 minutes stimulation with PDBu caused a dose-dependent increase in ERK2-GFP phosphorylation (whole cell ppERK2) and nuclear localization (ERK2-GFP N:C), and 6 hours stimulation caused a corresponding increase in Egr-1 Luc activity. All 3 responses were markedly reduced in cells expressing the non-TEY phosphorylatable T183/Y185A ERK2-GFP mutant, confirming the effectiveness of the mutation as well as the dependence of nuclear localization and nuclear signaling on TEY phosphorylation. PDBu also dose-dependently increased phosphorylation and nuclear localization of the K52R mutant, but the Egr-1 response was greatly reduced, demonstrating that activation of the transcription reporter requires ERK catalytic activity whereas the phosphorylation and nuclear localization responses do not (Gonzalez et al., 1993). Interestingly, the basal ppERK2 levels and ERK2-GFP N:C ratio were increased with this mutant (Fig. 7B), which may well reflect a lack of negative feedback requiring ERK catalytic activity (Catalanotti et al., 2009; Dougherty et al., 2005). The Y261A mutation, which inhibits DEF domain-dependent binding, did not affect ERK2-GFP phosphorylation in response to PDBu but did increase N:C ERK2-GFP ratios in basal and stimulated cells, and actually reduced PDBu-stimulated Egr-1 Luc activity (Fig. 7B). The latter effect is known to reflect dependence on DEF-directed phosphorylation and activation of immediate early gene transcription factors (Dimitri et al., 2005; Murphy et al., 2004; Murphy et al., 2002). In contrast, inhibition of ERK2 binding to D-domain partners (D319N mutation) did not affect ERK2-GFP phosphorylation, but substantially reduced nuclear localization and doubled Egr-1 Luc

responses (Fig. 6B). Together, these findings show that each of these biochemical motifs is necessary for correct regulation of ERK1/2 localization and downstream response, and confirm that effects of catalysis and docking interactions can be functionally separated *in vivo* using this system.

We next asked whether the uncoupling of ERK phosphorylation from nuclear localization seen with endogenous ERK would also be seen with the knock-down/add-back model. To do so, cells expressing endogenous ERK were stimulated for 5 minutes with 0, 0.1 or 1 µM PDBu before staining for ppERK1/2 and ERK1/2. Cells transduced with ERK2-GFP were treated similarly (except that the GFP fluorescence was used instead of total ERK1/2 staining) and the single cell data was binned according to ppERK1/2 level. In control cells expressing endogenous ERK the expected positive correlation between ppERK1/2 and ERK1/2 N:C, as was the marked uncoupling of responses (i.e. the PDBu-induced increase in ERK1/2 N:C in cell subsets with matched ppERK1/2 level). Very similar data were obtained in cells transduced with ERK2-GFP (Fig. 8).

The previous data show that the GFP tag does not interfere with the component of the nuclear localization response that cannot be attributed to TEY phosphorylation, and provided the opportunity to explore mechanisms using the ERK2-GFP mutants. Accordingly, we compared the effect of the ERK2-GFP mutants on stimulus-dependent localization within matched ppERK2 levels. This analysis clearly cannot be performed with the T183/Y185A mutant (which lacks the TEY phosphorylation epitope). As expected, there was clear uncoupling of nuclear localization from phosphorylation in cells expressing WT ERK2-GFP and stimulated for 5 min with 0.1 or 1 µM PDBu. Very similar data were obtained in cells expressing the K52R and Y261A mutants (Fig. 9A). In contrast, the uncoupling of phosphorylation from nuclear localization was much less pronounced in cells expressing D319N ERK2-GFP (Fig. 9A). This distinction was also evident in dose-response studies where data are plotted for the sub-set of cells within a single narrow ppERK2 bin (160-240 AFU). This revealed a clear dose-dependent increase in N:C ERK2-GFP under conditions where there was no measurable PDBu-stimulated increase in ppERK2 (Fig. 9B). The nuclear localization response seen with the binned data was greatly reduced in cells expressing D319N ERK2-GFP. Consistent with the population averaged data (Fig. 7) we also found that the K52R and Y261A mutants increased ERK2-GFP N:C ratios in the absence of stimulus and this was

additive with the PDBu effects. Together, these data demonstrate that there is an additional component of the nuclear localization response that cannot be attributed to TEY phosphorylation, does not require catalysis or DEF domain-dependent binding, but is largely prevented by the D319N mutation and therefore requires D-domain-dependent binding.

Discussion
The compartmentalization of ERK dictates substrate access and in turn controls cell fate decisions. ERK does not contain nuclear localization or export sequences, so its compartmentalization is determined largely by binding to scaffolds, anchors and substrates (Caunt et al., 2006a). In unstimulated cells ERK is mainly bound to MEK in the cytoplasm (Chuderland et al., 2008b; Fukuda et al., 1997). When MEK catalyses the TEY phosphorylation of ERK, this not only activates the enzyme but also causes its dissociation from MEK and exposes binding motifs enabling its interaction with other binding partners including components of the nuclear transport pore (Adachi et al., 1999; Lee et al. 2004; Wolf et al., 2001; Yazicioglu et al. 2007). The importance of MEK for cytoplasmic retention of ERK in unstimulated cells is illustrated by the characteristic redistribution of ERK from the cytoplasm to the nucleus seen when MEK is activated (Adachi et al., 1999; Chen et al., 1992; Lenormand et al., 1993). TEY phosphorylation of ERK may be insufficient for maximal stimulation of nuclear ERK localization as additional phosphorylation sites (Ser 244, Ser 246 and Thr 188) are also implicated in control of nuclear localization (Chuderland et al. 2008a; Lorenz et al. 2009). Moreover, ERK can be largely restricted to the cytoplasm by elevation of the cytoplasmic Ca^{2+} concentration which can inhibit its transport into the nucleus (Chuderland et al., 2008b) and by engaging signaling pathways in which β-arrestin binding retains ERK in the cytoplasm (Caunt et al., 2006b; Luttrell et al., 2001; Tohgo et al., 2002). Conversely, many activators of ERK also increase expression of nuclear-inducible DUSPs that can de-phosphorylate and anchor ERK, thereby increasing the proportion of ERK in the nucleus (Caunt et al., 2008a; Caunt et al., 2008b; Mandl et al., 2005; Volmat et al., 2001).

The data above illustrate the potential for uncoupling of ERK phosphorylation from nuclear localization, but most of the supporting evidence derives from studies of large cell populations (i.e. homogenates of cultured cells) or imaging of small numbers of cells. Here, we have developed a novel approach based on automated fluorescence microscopy to determine the relationship between ERK phosphorylation and

compartmentalization in large numbers of individual cells. A useful feature of this approach is that it enables the cells to be sorted (binned) into subpopulations according to ppERK1/2 level. Plotting ppERK1/2 level (bin mean) against nuclear:cytoplasmic (N:C) ERK1/2 ratio then provides a simple measure of the relationship between phosphorylation and nuclear localization, and also enables comparison of control and stimulated cells under conditions of matched ppERK1/2 level. This analysis revealed the expected positive correlation between ppERK1/2 and ERK1/2 N:C in control cells (Fig. 2B). We suspected that stimulation would simply extend this relationship, driving more cells into the higher ppERK1/2 bins and causing a corresponding increase in N:C ERK1/2. This is precisely what was seen when tyrosine phosphatases were inhibited with vanadate but the relationship between ppERK1/2 and N:C ERK1/2 was entirely different in cells treated with PDBu for 2 hr (Fig. 2B). Under this condition, increasing ppERK1/2 did not increase N:C ERK1/2 and importantly, the N:C ERK1/2 ratio was greater in PDBu-stimulated cells than in control cells in all ppERK1/2 bins. Thus, 2 hours exposure to PDBu causes two distinct effects; firstly, it increases TEY phosphorylation of ERK1/2, as evidenced by the increase ppERK1/2 seen in analysis of the whole cell population (Fig. 1) and by the increased mode value seen in frequency distribution plots (supplementary Fig. 1); secondly, it causes an increase in N:C ERK1/2 that is not attributable to the increased TEY phosphorylation, because it is seen under conditions matched for ppERK1/2 levels (Fig. 2B). Similar uncoupling (i.e. stimulus induced increases in N:C ERK1/2 with cells binned for indistinguishable ppERK1/2 levels) was seen at early time-points (5 minutes) and in 3 different cell types (HeLa, MCF7 and mouse embryonal fibroblasts) although in all cases it was less pronounced at 5 minutes (Fig. 2 and Supplemental Fig. 2).

To our knowledge this is the first study in which ppERK levels and ERK compartmentalisation have been related in large numbers of individual adherent cells (data herein derive from measures of ppERK2 and N:C ERK in several million individual cells). However, a key earlier study used flow cytometry to explore the issue of graded versus switch-like signalling in the ERK pathway (MacKeigan et al. 2005). This revealed that the PDGF-stimulated ppERK1/2 response in Swiss 3T3 fibroblasts was graded, whereas c-Fos induction was an all-or-nothing response at the individual cell level (MacKeigan et al. 2005). Since c-Fos induction was used as a readout for nuclear ERK activity it was

suggested that graded ERK phosphorylation stimulated all-or-nothing nuclear localization. This provides another potential explanation for uncoupling of ppERK1/2 and N:C ERK1/2 responses, if maximal nuclear localization occurred at low ppERK levels further increases in ppERK1/2 would have no effect on nuclear localization. However, this appears not to be the case in our model as we see graded responses to PDBu for both ERK phosphorylation and nuclear localization (Fig. 2). Moreover, any such relationship would be expected to yield a step-wise increase in binned data plots of ppERK1/2 against N:C ERK1/2, and no such increase was seen in control cells or in the presence of any of the stimuli used (Fig. 5). Interestingly, we observed graded N:C ERK1/2 and graded nuclear ppERK1/2 responses in HeLa and MCF7 cells (Fig. 2 and not shown) suggesting that where ERK drives switch-like down-stream responses (e.g. cell cycle entry and apoptosis) the transduction from graded to switch-like behaviour occurs distal to TEY phosphorylation and nuclear localization of ERK.

A key finding of this study is that the relationship between ppERK1/2 level and N:C ERK1/2 is entirely different between unstimulated and PDBu-stimulated cells (Fig. 2); namely, that PDBu has an effect on nuclear ERK1/2 localization beyond that simply attributable to TEY phosphorylation of ERK (Figs. 3 and 4). Since we have imaged fixed cells it is not possible to know whether PKC activation does so by altering ERK trafficking to or from the nucleus, or to effects on anchoring in the cytoplasm or nucleus. However, the uncoupling at later time points is most probably due to the PKC-mediated increase in expression of nuclear-inducible DUSPs (Caunt et al., 2008a; Caunt et al., 2008b). Nevertheless, this clearly cannot be the case for similar uncoupling seen in cells stimulated for only 5 minutes with PDBu (Figs. 2C, 3, 4 and Supplemental Fig. 2). In confirmation of this, the presence of protein synthesis or tyrosine phosphatase inhibitors failed to have any effect on PDBu-mediated ERK redistribution in HeLa cells at these early time points, but did effect signaling in sustained phases (Fig. 5, (Caunt et al., 2008a; Caunt et al., 2008b) and not shown). Thus, we have found a previously unidentified component of ERK signaling downstream of PKC; a TEY phosphorylation unattributable nuclear localization response that does not reflect PKC-induced expression of nuclear anchors. Indeed, our observation of an acute TEY phosphorylation unattributable nuclear localization response is not readily explained bu any of the above described mechanisms for uncoupling of TEY

phosphorylation from nuclear localization (Chuderland et al. 2008a; Chuderland et al. 2008b; Lorenz et al. 2009; Luttrell et al., 2001; Tohgo et al., 2002; Caunt et al., 2008a; Caunt et al., 2008b; Mandl et al., 2005; Volmat et al., 2001).

This additional component of PKC-mediated ERK nuclear localization was also seen using a knock-down/add-back model in which siRNAs are used to reduce expression of endogenous ERK and recombinant adenovirus are used to express ERK2-GFP reporters (Figs. 8 and 9). This enabled us to use pharmacological inhibitors to probe mechanisms in cells with endogenous ERK and mutated ERK2-GFP reporters to do so in the knock-down/add-back model. This revealed that the uncoupling of ERK phosphorylation from nuclear localization was prevented either by inhibition of MEK (PD184352) or by expression of a non-TEY phosphorylatable (T183/Y185A) mutant. Thus, the phosphorylation unattributable component of the response cannot be described as phosphorylation-independent. Instead, we show that MEK catalysed TEY phosphorylation of ERK is necessary, but not sufficient, for the full ERK nuclear localization response.

Comparison of cells treated with PDBu, EGF and vanadate revealed that the ERK nuclear localization response is governed by stimulus rather than phosphorylation levels. PDBu and EGF both caused phosphorylation unattributable nuclear localization of ERK (Fig. 4). The EGF response was not affected by a PKC inhibitor (Ro 31-8425), indicating that this component of the ERK nuclear localization response can be induced by more than just PKC activation (not shown). In contrast, vanadate was unable to cause this component of the nuclear localization response, despite causing robust increases in ERK phosphorylation (Fig. 4). These data reveal that simply increasing levels of phosphorylated ERK does not necessarily provoke this additional component of the nuclear localization response. Accordingly, they add to the growing body of evidence showing that compartmentalization of ERK is stimulus-specific (von Kriegsheim et al., 2009; Whitehurst et al., 2004).

In contrast to mutation of the TEY motif, we found that inhibition of catalysis (using a K52R mutation) or inhibition of DEF-domain binding (using a Y261A mutation) increased nuclear localization of ERK2-GFP in basal and stimulated cells. This was true in both average cell populations and in matched phosphorylation bins (Figs. 7B and 9). This could be because K52R ERK2-GFP is not retained in the cytosol, as suggested by studies showing the K52R mutant inhibits ERK traffic to the ruffling membrane

but not the nucleus (Gonzalez et al., 1993; Yazicioglu et al., 2007). Previous studies have also implicated DEF-domain interactions in basal nuclear traffic of ERK (Casar et al., 2007), but exactly why K52R or Y261A mutants distinguish basal from stimulus-regulated ERK2-GFP localization patterns is currently unclear. More importantly in the context of this study however, we were able to establish that neither mutation significantly affected the phosphorylation unattributable component of the ERK nuclear localization response (Fig. 9).

Intriguingly, we found that reduction of D-domain binding (using a D319N mutation) not only inhibited 5 minutes PDBu or EGF-induced nuclear accumulation of ERK2-GFP (Fig. 7B and not shown), but also removed the phosphorylation unattributable component of the nuclear localization response (Fig. 9). Thus, PKC and EGFR both activate pathways causing regulation of an unidentified D-domain containing protein (or proteins) that is/are required for the full ERK nuclear localization response. In spite of this, the D319N mutation actually increased PDBu-stimulated Egr-1-luc activity, demonstrating the overriding importance of D-domain containing phosphatases in terminating sustained ERK signaling (Caunt et al., 2008a; Caunt et al., 2008b; Mandl et al., 2005; Volmat et al., 2001). Clearly, more specific methods will be needed to explore this additional component of the localization response without perturbation of ERK binding to phosphatases and we are currently focusing on identifying specific D-domain containing ERK binding partners in this model.

Taken together, we show that phosphorylation of ERK by MEK on the TEY motif is necessary but not sufficient for the full nuclear localization response to occur. Instead, there is an additional TEY phosphorylation unattributable component of the ERK translocation response that is provoked by PKC or EGFR activation and does not reflect induced expression of nuclear anchors. We also show that this component of the response is not dependent on ERK catalytic activity or DEF-domain association, but is reliant on binding to stimulus-regulated D-domain containing proteins. These studies illustrate how spatially distinct ERK domains control functionally separate aspects of stimulus-regulated subcellular targeting, and will ultimately inform identification of candidate binding partners responsible for these different modes of regulation.

Materials and Methods
Engineering of Plasmids and Viruses

Viral shuttle vectors were constructed initially by subcloning a *Kpn*I-*Not*I digest of ERK2-GFP in pEGFP-N1 (a gift from Prof. Louis Luttrell, Medical University of South Carolina, Charleston, USA) into a corresponding digest of pacAd5CMV K-N pA (donated by Prof. Beverly Davidson, University of Iowa, Iowa City, USA). K52R, T183/Y185A, Y261A and D319N mutations were introduced using a QuikChange PCR-based mutagenesis kit (Stratagene, Amsterdam, NL) and the following primers: 5'-CAA AGT TCG AGT TGC TAT CAG GAA AAT CAG TCC TTT TGA GC-3', 5'-TGA TCA TAC AGG GTT CTT GGC AGA GGC TGT AGC CAC GCG TTG GTA C-3', 5'-AAT TTA AAA GCT AGA AAC GCT TTG CTT TCT CTC CCG CAC-3' and 5'-GCA GTA TTA TGA CCC AAG TAA TGA GCC CAT GC TGA AGC-3' along with antisense primers according to manufacturer's recommendations and using the pacAd5CMV ERK2-GFP vector as the template. Ad Egr-1 Luciferase and Ad CMV β-galactosidase reporter shuttle vectors were constructed as described (Caunt et al., 2008a; Armstrong et al. 2010). Viruses were generated from shuttle vectors as described (Anderson et al., 2000; Caunt et al., 2006b). Briefly, 4.5µg of shuttle vectors were digested alongside 1.5µg of pacAd5 9.2-100 sub360 backbone vector (kindly donated by Prof. Beverly Davidson, University of Iowa, Iowa City, USA) with *Pac*I. Cut shuttle and backbone vectors were then mixed and transfected into low passage HEK293 cells using Superfect (Qiagen, Crawley, UK). Cells were left to allow recombination between shuttle and backbone vectors. Verification of recombination was performed by restriction digest and sequence analysis, and Ad vectors were grown to high titre and purified according to standard protocols.

Cell Culture and Transfection
HeLa and MCF7 cells (from ECACC) were cultured in 10% FCS-supplemented Dulbecco's modified Eagle's medium (DMEM) without sodium pyruvate. Mouse embryonal fibroblasts (a kind gift from Prof Stephen Keyse, University of Dundee, UK) were cultured in 10% FCS-supplemented DMEM with sodium pyruvate. For 96-well plate experiments, cells were harvested by trypsinization and seeded at $3-5 \times 10^3$ cells/well. Where necessary, cells were transfected using RNAiMAX reagent (Invitrogen, Paisley, UK) and the manufacturer's reverse transfection protocol. Cells were transfected with 2 siRNA duplexes (Qiagen) each for ERK1: 5'-CGU CUA AUA UAU AAA UAU AdTdT-3', 5'-UAU AUU UAU AUA UUA GAC GdGdG-3' and 5'-CCC UGA CCC GUC UAA UAU AdTdT-3', 5'-UAU AUU AGA CGG GUC AGG GdAdG-3' and for ERK2: 5'-CAC UUG UCA AGA AGC GUU AdTdT-3', 5'-UAA CGC UUC UUG ACA AGU GdTdT-3' and 5'-CAU GGU AGU CAC UAA CAU AdTdT-3', 5'-UAU GUU AGU GAC UAC CAU GdAdT-3' which have been validated in recent publications (Caunt et al., 2008a; Caunt et al., 2008b; Dimitri et al., 2005). A mixture of all 4 ERK1/2 duplexes or control siRNA against GFP (Ambion, Warrington, UK) was used in experiments at 2.5 nM total concentrations. Sixteen hours after siRNA transfection, cells were transduced with 0 or 1.5×10^6 plaque-forming units (pfu)/ml Ad WT, K52R, T183/Y185A, Y261A or D319N ERK2-GFP vector in DMEM with 10% FCS. The Ad-containing medium was removed after 4–6 hours and replaced with fresh DMEM supplemented with 0.1% FCS. The cells were then maintained for 16–24 h in culture prior to stimulation with GnRH EGF (Calbiochem, San Diego, CA, USA), PDBu (phorbol 12, 13-dibutyrate, Sigma) or sodium orthovanadate (Sigma). In some experiments, cells were treated with 10 µM PD184352 (Enzo Life Sciences, Exeter, UK), 200 nM Ro31-8425 (Roche, Welyn Garden City, UK) 30µM cycloheximide (Sigma) or 1mM sodium orthovanadate (Sigma) for 10 min prior to stimulation. Expression levels of GFP-tagged fusions were compared using western blotting techniques (see Fig. 6A) as well as comparison of mean cell fluorescence in microscopy assays.

Western Blotting
HeLa cells were plated in 6-well plates at 2.5×10^5 cells/well. Where required, cells were transfected with 2.5 nM ERK1/2 siRNAs prior to Ad transduction as above. Following treatment noted in figure legends, cells were lysed as described, prior to western blotting. Total and ppERK1/2 were detected using rabbit anti-ERK1/2 monoclonal (clone 137F5, 1:1000; Cell Signaling Technology, Hitchin, UK) and mouse anti-ppERK1/2 monoclonal antibody (clone MAPK-YT, 1:2000, Sigma), respectively. Total and Ser217/221 phosphorylated MEK1/2 were detected using rabbit anti-MEK1/2 monoclonal (clone 47E6, 1:1000, Cell Signaling Technology) and rabbit anti-ppMEK1/2 monoclonal (clone 41G9, 1:1000, Cell Signaling Technology), respectively. DUSP1 was detected using rabbit anti-DUSP1 polyclonal (M-18, 1:500, Santa Cruz Biotechnology, CA USA). Antibodies were visualized using horseradish peroxidase linked secondary antibody and enhanced chemiluminescence kit (GE Healthcare, Amersham, UK).

High-content Image Acquisition and Analysis
Cells were plated (and transfected with siRNA, and Ad vectors as necessary) as described above on Costar plain black-wall 96-well plates (Corning, Arlington, UK) prior to treatment as noted in figure legends. Cells were fixed in 4% paraformaldehyde/PBS and permeabilized in -20˚C methanol. After blocking in 5% normal goat

serum/PBS, cells were probed with mouse anti-ppERK1/2 monoclonal antibody (clone MAPK-YT, 1:200, Sigma) and rabbit anti-ERK1/2 monoclonal (clone 137F5, 1:100, Cell Signaling Technology) in PBS. Alexa 488-conjugated goat anti-mouse and Alexa 546-conjugated goat anti-rabbit secondary antibodies (1:200, Invitrogen) and DAPI/PBS (600nM) were used to visualize ppERK1/2, ERK1/2 antibodies and stain nuclei, respectively in imaging of endogenous kinases. For imaging cells transduced with Ad ERK2-GFP, cells were counterstained with rabbit anti-ERK1/2 monoclonal (1:100) and Alexa 546-conjugated goat anti-rabbit secondary (1:200) for assessing expression levels and setting filter levels (to ensure only ERK2-GFP expressing cells within physiological ranges were included in analysis in subsequent assays). For imaging ppERK2 in cells expressing ERK2-GFP, cells were counterstained with mouse anti ppERK1/2 monoclonal (1:200) and Alexa 546-conjugated goat anti mouse secondary (1:200) as above. Image acquisition in each well was performed on an IN Cell Analyzer 1000 (GE Healthcare) microscope, using a x10 objective and 360nm (DAPI), 475nm (Alexa 488 and GFP) and 535nm (Alexa 546) excitation filters, and monitored through 460nm, 535nm and 620nm emission filters, respectively, with a 61002 trichroic mirror (GE Healthcare). Analysis of endogenous ERK1/2 and ppERK1/2 was performed using the Multi-target Analysis algorithm and "region growing" cell identification module in the IN Cell Analyzer Workstation (GE Healthcare) using DAPI and ERK1/2 stained images to define nuclear and cytoplasmic regions, respectively, which were used as a mask for detection of changes in ppERK1/2 staining. ERK2-GFP and ERK1/2 or ppERK1/2 stained cells were similarly analysed using the Multi-target Analysis algorithm, but using the more sensitive "multiscale top hat" cell identification module (IN Cell Analyzer Workstation, GE Healthcare). In both ppERK2 and GFP readouts, cells expressing sub- or super-physiological levels of ERK2-GFP were excluded from analysis (based on comparisons of frequency histograms of ERK1/2 staining intensity in cells transfected with Ctrl siRNA, ERK1/2 siRNAs and with ERK1/2 siRNAs plus Ad ERK2-GFP). Mitotic and apoptotic nuclei were excluded from analysis, as were aberrantly identified cells using a "decision tree" filter based on multiple readouts of intensity and shape defined in nuclear and cellular regions. Imaging data are reported as ppERK1/2 intensity (mean fluorescence intensity per cell) or as a ratio of nuclear to cytoplasmic stain intensity (N:C ratio). Sorting of cells into linked subpopulations according to ppERK1/2 staining intensity was performed using a macro in Microsoft Excel (kindly designed by Neil Rich, University of Bristol, UK).

Luciferase Assays

Cells were transfected with siRNA, transduced with Ad vectors and plated as described above on Costar plain black-wall 96-well plates (Corning), but including Ad Egr-1 Luciferase and Ad CMV β-galactosidase reporter vectors. Following treatment with PDBu, cells were washed in ice-cold PBS, lysed and assessed for luciferase activity by chemical luminescence following the addition of luciferin substrate (Promega, Southampton, UK). β-galactosidase activity was used to correct luciferase activity for transfection efficiency, as measured following the addition of chlorophenol red-β-D-galactopyranoside substrate (Roche).

References

Adachi, M., Fukuda, M. and Nishida, E. (1999). Two co-existing mechanisms for nuclear import of MAP kinase: passive diffusion of a monomer and active transport of a dimer. *EMBO J* **18**, 5347-58.

Anderson, R. D., Haskell, R. E., Xia, H., Roessler, B. J. and Davidson, B. L. (2000). A simple method for the rapid generation of recombinant adenovirus vectors. *Gene Ther* **7**, 1034-8.

Armstrong, S. P., Caunt, C. J., Fowkes, R. C., Tsaneva-Atanasova, K. and McArdle, C. A. (2010). Pulsatile and sustained gonadotropin-releasing hormone (GnRH) receptor signaling: Does the ERK signaling pathway decode GnRH pulse frequency? *J Biol Chem* **32**, 24360-71

Brunet, A., Roux, D., Lenormand, P., Dowd, S., Keyse, S. and Pouyssegur, J. (1999). Nuclear translocation of p42/p44 mitogen-activated protein kinase is required for growth factor-induced gene expression and cell cycle entry. *EMBO J* **18**, 664-74.

Casar, B., Sanz-Moreno, V., Yazicioglu, M. N., Rodriguez, J., Berciano, M. T., Lafarga, M., Cobb, M. H. and Crespo, P. (2007). Mxi2 promotes stimulus-independent ERK nuclear translocation. *EMBO J* **26**, 635-46.

Catalanotti, F., Reyes, G., Jesenberger, V., Galabova-Kovacs, G., de Matos Simoes, R., Carugo, O. and Baccarini, M. (2009). A Mek1-Mek2 heterodimer determines the strength and duration of the Erk signal. *Nat Struct Mol Biol* **16**, 294-303.

Caunt, C. J., Armstrong, S. P., Rivers, C. A., Norman, M. R. and McArdle, C. A. (2008a). Spatiotemporal regulation of ERK2 by dual specificity phosphatases. *J Biol Chem* **283**, 26612-23.

Caunt, C. J., Finch, A. R., Sedgley, K. R. and McArdle, C. A. (2006a). Seven-transmembrane receptor signalling and ERK compartmentalization. *Trends Endocrinol Metab* **17**, 276-83.

Caunt, C. J., Finch, A. R., Sedgley, K. R., Oakley, L., Luttrell, L. M. and McArdle, C. A. (2006b). Arrestin-mediated ERK activation by gonadotropin-releasing hormone receptors: receptor-specific activation mechanisms and compartmentalization. *J Biol Chem* **281**, 2701-10.

Caunt, C. J., Rivers, C. A., Conway-Campbell, B. L., Norman, M. R. and McArdle, C. A. (2008b). Epidermal growth factor receptor and protein kinase C signaling to ERK2: spatiotemporal regulation of ERK2 by dual specificity phosphatases. *J Biol Chem* **283**, 6241-52.

Chen, R. H., Sarnecki, C. and Blenis, J. (1992). Nuclear localization and regulation of erk- and rsk-encoded protein kinases. *Mol Cell Biol* **12**, 915-27.

Chuderland, D., Konson, A. and Seger, R. (2008a). Identification and characterization of a general nuclear translocation signal in signaling proteins. *Mol Cell* **31**, 850-61.

Chuderland, D., Marmor, G., Shainskaya, A. and Seger, R. (2008b). Calcium-mediated interactions regulate the subcellular localization of extracellular signal-regulated kinases. *J Biol Chem* **283**, 11176-88.

Costa, M., Marchi, M., Cardarelli, F., Roy, A., Beltram, F., Maffei, L., Ratto, G. M. (2006). Dynamic regulation of ERK2 nuclear translocation and mobility in living cells. *J Cell Sci* **119**, 4952-63.

Dimitri, C. A., Dowdle, W., MacKeigan, J. P., Blenis, J. and Murphy, L. O. (2005). Spatially separate docking sites on ERK2 regulate distinct signaling events in vivo. *Curr Biol* **15**, 1319-24.

Dougherty, M. K., Muller, J., Ritt, D. A., Zhou, M., Zhou, X. Z., Copeland, T. D., Conrads, T. P., Veenstra, T. D., Lu, K. P. and Morrison, D. K. (2005). Regulation of Raf-1 by direct feedback phosphorylation. *Mol Cell* **17**, 215-24.

Ferrell, J. E., Jr. and Machleder, E. M. (1998). The biochemical basis of an all-or-none cell fate switch in Xenopus oocytes. *Science* **280**, 895-8.

Formstecher, E., Ramos, J. W., Fauquet, M., Calderwood, D. A., Hsieh, J. C., Canton, B., Nguyen, X. T., Barnier, J. V., Camonis, J., Ginsberg, M. H., Chneiweiss, H. (2001). PEA-15 mediates cytoplasmic sequestration of ERK MAP kinase. *Dev Cell* **1**, 239-50

Fukuda, M., Gotoh, Y. and Nishida, E. (1997). Interaction of MAP kinase with MAP kinase kinase: its possible role in the control of nucleocytoplasmic transport of MAP kinase. *EMBO J* **16**, 1901-8.

Gonzalez, F. A., Seth, A., Raden, D. L., Bowman, D. S., Fay, F. S. and Davis, R. J. (1993). Serum-induced translocation of mitogen-activated protein kinase to the cell surface ruffling membrane and the nucleus. *J Cell Biol* **122**, 1089-101.

Jacobs, D., Glossip, D., Xing, H., Muslin, A. J. and Kornfeld, K. (1999). Multiple docking sites on substrate proteins form a modular system that mediates recognition by ERK MAP kinase. *Genes Dev* **13**, 163-75.

Karlsson, M., Mathers, J., Dickinson, R. J., Mandl, M. and Keyse, S. M. (2004). Both nuclear-cytoplasmic shuttling of the dual specificity phosphatase MKP-3 and its ability to anchor MAP kinase in the cytoplasm are mediated by a conserved nuclear export signal. *J Biol Chem* **279**, 41882-91.

Khokhlatchev, A. V., Canagarajah, B., Wilsbacher, J., Robinson, M., Atkinson, M., Goldsmith, E. and Cobb, M. H. (1998). Phosphorylation of the MAP kinase ERK2 promotes its homodimerization and nuclear translocation. *Cell* **93**, 605-15.

Lee, T., Hoofnagle, A. N., Kabuyama, Y., Stroud, J., Min, X., Goldsmith, E. J., Chen, L., Resing, K. A. and Ahn, N. G. (2004). Docking motif interactions in MAP kinases revealed by hydrogen exchange mass spectrometry. *Mol Cell* **14**, 43-55.

Lenormand, P., Brondello, J. M., Brunet, A. and Pouyssegur, J. (1998). Growth factor-induced p42/p44 MAPK nuclear translocation and retention requires both MAPK activation and neosynthesis of nuclear anchoring proteins. *J Cell Biol* **142**, 625-33.

Lenormand, P., Sardet, C., Pages, G., L'Allemain, G., Brunet, A. and Pouyssegur, J. (1993). Growth factors induce nuclear translocation of MAP kinases (p42mapk and p44mapk) but not of their activator MAP kinase kinase (p45mapkk) in fibroblasts. *J Cell Biol* **122**, 1079-88.

Lidke, D. S., Huang, F., Post, J. N., Rieger, B., Wilsbacher, J., Thomas, J. L., Pouyssegur, J., Jovin, T. M. and Lenormand, P. (2010). ERK nuclear translocation is dimerization-independent but controlled by the rate of phosphorylation. *J Biol Chem* **285**, 3092-102.

Lin, J., Harding, A., Giurisato, E. and Shaw, A. S. (2009). KSR1 modulates the sensitivity of mitogen-activated protein kinase pathway activation in T cells without altering fundamental system outputs. *Mol Cell Biol* **29**, 2082-91.

Lorenz, K., Schmitt, J.P., Schmitteckert, E.M., Lohse, M.J. (2009) A new type of ERK1/2 autophosphorylation causes cardiac hypertrophy. *Nat Med* **15**, 75-83

Luttrell, L. M., Roudabush, F. L., Choy, E. W., Miller, W. E., Field, M. E., Pierce, K. L. and Lefkowitz, R. J. (2001). Activation and targeting of extracellular signal-regulated kinases by beta-arrestin scaffolds. *Proc Natl Acad Sci U S A* **98**, 2449-54.

Mackeigan, J. P., Murphy, L. O., Dimitri, C. A. and Blenis, J. (2005). Graded mitogen-activated protein kinase activity precedes switch-like c-Fos induction in mammalian cells. *Mol Cell Biol* **25**, 4676-82.

Mandl, M., Slack, D. N. and Keyse, S. M. (2005). Specific inactivation and nuclear anchoring of extracellular signal-regulated kinase 2 by the inducible dual-specificity protein phosphatase DUSP5. *Mol Cell Biol* **25**, 1830-45.

Murphy, L. O., MacKeigan, J. P. and Blenis, J. (2004). A network of immediate early gene products propagates subtle differences in mitogen-activated protein kinase signal amplitude and duration. *Mol Cell Biol* **24**, 144-53.

Murphy, L. O., Smith, S., Chen, R. H., Fingar, D. C. and Blenis, J. (2002). Molecular interpretation of ERK signal duration by immediate early gene products. *Nat Cell Biol* **4**, 556-64.

Raman, M., Chen, W. and Cobb, M. H. (2007). Differential regulation and properties of MAPKs. *Oncogene* **26**, 3100-12.

Robinson, F. L., Whitehurst, A. W., Raman, M. and Cobb, M. H. (2002). Identification of novel point mutations in ERK2 that selectively disrupt binding to MEK1. *J Biol Chem* **277**, 14844-52.

Robinson, M. J., Stippec, S. A., Goldsmith, E., White, M. A. and Cobb, M. H. (1998). A constitutively active and nuclear form of the MAP kinase ERK2 is sufficient for neurite outgrowth and cell transformation. *Curr Biol* **8**, 1141-50.

Shin, S., Dimitri, C. A., Yoon, S. O., Dowdle, W. and Blenis, J. (2010). ERK2 but not ERK1 induces epithelial-to-mesenchymal transformation via DEF motif-dependent signaling events. *Mol Cell* **38**, 114-27.

Tanoue, T., Maeda, R., Adachi, M. and Nishida, E. (2001). Identification of a docking groove on ERK and p38 MAP kinases that regulates the specificity of docking interactions. *EMBO J* **20**, 466-79.

Tohgo, A., Pierce, K. L., Choy, E. W., Lefkowitz, R. J. and Luttrell, L. M. (2002). beta-Arrestin scaffolding of the ERK cascade enhances cytosolic ERK activity but inhibits ERK-mediated transcription following angiotensin AT1a receptor stimulation. *J Biol Chem* **277**, 9429-36.

Torii, S., Kusakabe, M., Yamamoto, T., Maekawa, M. and Nishida, E. (2004). Sef is a spatial regulator for Ras/MAP kinase signaling. *Dev Cell* **7**, 33-44.

Volmat, V., Camps, M., Arkinstall, S., Pouyssegur, J. and Lenormand, P. (2001). The nucleus, a site for signal termination by sequestration and inactivation of p42/p44 MAP kinases. *J Cell Sci* **114**, 3433-43.

von Kriegsheim, A., Baiocchi, D., Birtwistle, M., Sumpton, D., Bienvenut, W., Morrice, N., Yamada, K., Lamond, A., Kalna, G., Orton, R. et al. (2009). Cell fate decisions are specified by the dynamic ERK interactome. *Nat Cell Biol* **11**, 1458-64.

Whitehurst, A., Cobb, M. H. and White, M. A. (2004). Stimulus-coupled spatial restriction of extracellular signal-regulated kinase 1/2 activity contributes to the specificity of signal-response pathways. *Mol Cell Biol* **24**, 10145-50.

Whitehurst, A. W., Wilsbacher, J. L., You, Y., Luby-Phelps, K., Moore, M. S., Cobb, M. H. (2002). ERK2 enters the nucleus by a carrier-independent mechanism. *Proc Natl Acad Sci U S A* **99**, 7496-501

Wolf, I., Rubinfeld, H., Yoon, S., Marmor, G., Hanoch, T. and Seger, R. (2001). Involvement of the activation loop of ERK in the detachment from cytosolic anchoring. *J Biol Chem* **276**, 24490-7.

Yazicioglu, M. N., Goad, D. L., Ranganathan, A., Whitehurst, A. W., Goldsmith, E. J. and Cobb, M. H. (2007). Mutations in ERK2 binding sites affect nuclear entry. *J Biol Chem* **282**, 28759-67.

Figure Legends

Figure 1 Spatiotemporal characteristics of PDBu-stimulated ERK regulation in cell populations.
HeLa cells were seeded in 96-well imaging plates and kept in reduced (0.1%) serum for 16 hours prior to addition of 1 μM PDBu as indicated. (**A**) Cells were fixed and stained for endogenous ppERK1/2, ERK1/2 and DAPI before image acquisition and analysis (as described in Materials and Methods). Representative images of single fields of cells (left panels) and magnified areas of fields to show changes in subcellular localization (right panels) are shown. Outlines denote the segmentation of cells according to DAPI and ERK1/2 staining using IN Cell Analyzer software for the calculation of whole-cell ppERK1/2 intensity and N:C ERK1/2 ratio shown in (B). (**B**) Nine images per well, per fluorophore were acquired from cells in duplicate wells after PDBu treatment as indicated. Graphs represent population average values for ppERK1/2 intensity (left panel) and ERK1/2 N:C ratio (right panel) derived from 4 separate experiments (approx. 15,000-18,000 individual cells per condition) ±SEM. (**C**) Whole cell lysates of HeLa cells treated with PDBu were immunoblotted for phospho Ser217/221 MEK1/2 (ppMEK1/2), phospho Thr183/Tyr185 ERK1/2 (ppERK1/2), ERK1/2 and DUSP1 as indicated.

Figure 2 Uncoupling of ERK phosphorylation from nuclear localization.
(**A**) HeLa cells were seeded in 96-well imaging plates and kept in reduced (0.1%) serum for 16 hours prior to addition of 0 (Ctrl), 0.1 or 1 μM PDBu for 5 minutes as indicated. Cells were fixed and stained for ppERK1/2, ERK1/2 and DAPI before image acquisition and analysis (as described in Fig. 1). Frequency histograms of individual cells were plotted (pooled from 2 independent experiments) according to ppERK1/2 staining intensity (top panel) and ERK1/2 N:C ratio (bottom panel) from the same cell population in both graphs. (**B**) Cells were treated with 1 μM PDBu for 0 (Ctrl), 5 or 120 minutes as indicated before fixation, imaging and analysis as described in Fig. 1. In order to directly compare ppERK1/2 levels to ERK1/2 N:C, individual cells were sorted into bins of ppERK1/2 staining intensity (80 AFU per bin, using a minimum bin size of 50 cells per experiment). The average ERK1/2 N:C ratio within each defined bin of ppERK1/2 staining intensity was calculated and is shown plotted against average ppERK1/2 stain intensity. Data are shown from 6 separate experiments ±SEM. Note that this plot effectively obscures the effect of the stimulus on ERK phosphorylation because the major effect of PDBu is to increase the number of cells in the higher ppERK1/2 bins (and this is not evident in the figure). In doing so it reveals the TEY phosphorylation unattributable effect of PDBu: that is, the increase in ERK1/2 N:C under conditions matched for indistinguishable ppERK1/2 levels.

Figure 3 ERK nuclear localization is proportional to stimulus but not phosphorylation levels.
HeLa cells were seeded in 96-well imaging plates and kept in reduced (0.1%) serum for 16 hours prior to addition of increasing concentrations of PDBu as indicated for 5 minutes. Cells were fixed and stained for ppERK1/2, ERK1/2 and DAPI before image acquisition and analysis (as described in Fig. 1). (**Top panel**) The graph represents population average values for ppERK1/2 intensity (right y-axis) and ERK1/2 N:C ratio (left y-axis). (**Bottom panel**) This plot shows the same time-course as in (A), comparing ERK1/2 N:C ratio (left y-axis) only cells within a comparable range (240-320 AFU) of ppERK1/2 staining intensity (right y-axis). Data are shown from 6 separate experiments ±SEM. **= p<0.01, comparing control and PDBu-stimulated conditions for each readout, according to one-way ANOVA and Dunnet's post-hoc test.

Figure 4 Stimulus-induced changes in ERK localization occur at matched levels of phosphorylation.
HeLa cells were seeded in 96-well imaging plates and kept in reduced (0.1%) serum for 16 hours prior to addition of 1 μM PDBu for the times indicated. Cells were fixed and stained for ppERK1/2, ERK1/2 and DAPI before image acquisition and analysis (as described in Fig. 1). (**A**) The graph represents population average values for ppERK1/2 intensity (right y-axis) and ERK1/2 N:C ratio (left y-axis) derived from 3 separate experiments ±SEM. (**B**) This plot shows the same time-course as in (A), comparing ERK1/2 N:C ratio (left y-axis) only cells within a comparable range (240-320 AFU) of ppERK1/2 staining intensity (right y-axis). Data are shown from 3 separate experiments ±SEM.

Figure 5 The relationship between ERK phosphorylation and nuclear localization is stimulus specific.
HeLa cells were seeded in 96-well imaging plates and kept in reduced (0.1%) serum for 16 hours prior to addition of 1 μM PDBu, 10 nM EGF or 1 mM sodium orthovanadate (vanadate) for the times indicated. Cells were fixed and stained for ppERK1/2, ERK1/2 and DAPI before image acquisition and analysis (as

described in Fig. 1). (**A**) The graph represents population average values for ppERK1/2 intensity (right y-axis) and ERK1/2 N:C ratio (left y-axis) derived from 3 separate experiments ±SEM. (**B**) The plots represent the average ERK1/2 N:C ratio in cell populations stimulated with vehicle (Ctrl) or stimulated for 5 minutes (EGF and PDBu) or 3 hours (vanadate) within defined bins of ppERK1/2 staining intensity (80 AFU per bin, accepting a minimum of 50 cells per bin in each experiment). Data are shown from 3 separate experiments ±SEM.

Figure 6 Uncoupling of ERK phosphorylation from nuclear localization requires MEK activity.
HeLa cells were seeded in 96-well imaging plates and kept in reduced (0.1%) serum for 16 hours prior to addition of vehicle (Ctrl) 200 nM Ro31-8425 PKC inhibitor, 10 µM PD184352 MEK inhibitor, 200 nM SU6656 Src inhibitor, 1 mM sodium orthovanadate (vanadate) tyrosine phosphatase inhibitor or 30 µM cycloheximide (CHX) protein synthesis inhibitor for 10 minutes as indicated. Cells were then treated with 0-10 µM PDBu for 5 minutes prior to fixation and staining for ppERK1/2, ERK1/2 and DAPI before image acquisition and analysis (as described in Fig. 1). (**A**) The histograms show population average values for ppERK1/2 and ERK1/2 N:C after treatment with inhibitors and either vehicle (Ctrl) or 1 µM PDBu as indicated. Data are shown from 3 separate experiments ±SEM. **= $p<0.01$, comparing Ctrl and PDBu-stimulated conditions with inhibitor co-incubations for each readout, according to one-way ANOVA and Dunnet's post-hoc test. (**B**) The graphs represent full dose-response curves of ERK1/2 N:C ratio after treatment, comparing only cells within a comparable range (240-320 AFU) of ppERK1/2 staining intensity. Data are shown from 3 separate experiments ±SEM. **= $p<0.01$, comparing Ctrl and inhibitor-treated curves using two-way ANOVA and Bonferroni post-hoc tests

Figure 7 Phosphorylation, catalysis and docking domains influence ERK2-GFP localization and signaling.
(**A**) HeLa cells transfected with control siRNAs (Ctrl) or ERK1/2 siRNAs were transduced with Ad wild-type (WT), K52R, T183/Y185A, Y261A or D319N-mutated ERK2-GFP as indicated and stimulation with vehicle (-) or 1 µM PDBu (+) for 5 minutes before lysis. ERK1/2, MEK1/2 and ppMEK1/2 were assessed by immunoblotting of whole cell lysates as indicated. Densitometry (n=3) reveals >95% knock-down of ERK1/2 in control and PDBu stimulated cells in all Ad ERK2-GFP conditions with no significant effect on MEK expression or phosphorylation. (**B**) Cells transfected and transduced as described in (A) were stimulated for 5 minutes with indicated concentrations of PDBu before fixation, ppERK2 staining, image acquisition and analysis as described in Materials and Methods to assess whole-cell levels of ppERK2-GFP phosphorylation (ppERK2, top panel) and nucleo-cytoplasmic distribution of ERK2-GFP (ERK2-GFP N:C, middle panel). For Egr-1 luciferase assays, Ad Egr-1 luciferase and Ad CMV β-galactosidase vectors were also added to cells before stimulation with PDBu for 6h and assay of luciferase activity (Egr-1 Luc), and are expressed as fold induction (bottom panel). Data are shown from 3 separate experiments ±SEM. *= $p<0.05$ and **= $p<0.01$, comparing WT to mutant conditions, according to two-way ANOVA and Bonferroni post-hoc tests.

Figure 8 Uncoupling of endogenous ERK phosphorylation from nuclear localization is replicated in ERK2-GFP expressing cells.
Non-transfected HeLa cells (left panel), and HeLa cells transfected with ERK1/2 siRNAs and transduced with Ad WT ERK2-GFP (right panel) were treated with vehicle (Ctrl), 0.1 or 1 µM PDBu for 5 minutes prior to staining, imaging and analysis as described in Materials and Methods. The plots show comparison of average ERK1/2 N:C ratio in cell populations within defined bins of ppERK1/2 staining intensity (80 AFU per bin, accepting a minimum of 50 cells per bin in each experiment). Data are shown from 3 separate experiments ±SEM.

Figure 9 D319N mutation of ERK2-GFP inhibits stimulus-induced nuclear localization that is not attributable to increases in TEY phosphorylation.
(**A**) HeLa cells transfected with ERK1/2 siRNAs were transduced with Ad wild-type (WT), K52R, Y261A or D319N-mutated ERK2-GFP as indicated and stimulation with vehicle (Ctrl), 0.1 or 1 µM PDBu for 5 minutes prior to staining for ppERK2 and DAPI. Imaging and analysis was carried out as described in Materials and Methods. The plots show comparison of average ERK1/2 N:C ratio in cell populations within defined bins of ppERK1/2 staining intensity (80 AFU per bin, accepting a minimum of 50 cells per bin in each experiment). Data are shown from 3 separate experiments ±SEM. (**B**) The graphs show a full dose-response curves of ERK2-GFP N:C ratio (bottom panel) for cells transfected and transduced as described in

(A) and stimulated for 5 minutes with PDBu, comparing only cells within a comparable range (160-240 AFU) of ppERK1/2 staining intensity (top panel). Data are shown from 3 separate experiments ±SEM. *= p<0.05 and **= p<0.01, comparing WT to mutant conditions, according to two-way ANOVA and Bonferroni post-hoc tests.

Supplementary Figure 1 Time-course of stimulus-induced uncoupling of ERK phosphorylation from nuclear localization.
HeLa cells were seeded in 96-well imaging plates and kept in reduced (0.1%) serum for 16 hours prior to addition of 1 µM PDBu as indicated for 5-360 minutes. Cells were fixed and stained for ppERK1/2, ERK1/2 and DAPI before image acquisition and analysis (as described in Fig. 1). Cell populations pooled from 3 independent experiments were sorted into frequency histograms of ppERK1/2 staining intensity (left panels) and ERK1/2 N:C ratio (middle panels). To compare ppERK1/2 to ERK1/2 N:C ratio, cells were sorted into cell subpopulations (bins) of defined ppERK1/2 staining intensity (80 AFU per bin), before calculating the average ERK1/2 N:C value within each bin (using a minimum of 50 cells per bin, as described in Fig. 2B). The graphs are plotted as average ERK1/2 ratio against ppERK1/2 staining intensity within each 80 AFU bin. Data are shown from 3 separate experiments ±SEM

Supplementary Figure 2 Stimulus-induced uncoupling of ERK phosphorylation from nuclear localization in MCF7 and primary mouse embryo fibroblast cells.
MCF7 cells (**A-D**) and primary mouse embryo fibroblasts (**E-H**) were seeded in 96-well imaging plates and kept in reduced (0.1%) serum for 16 hours prior to addition of 1 µM PDBu as indicated for 5-360 minutes. Cells were fixed and stained for ppERK1/2, ERK1/2 and DAPI before image acquisition and analysis (as described in Fig. 1). (**A** and **E**) Graphs represent population average values for ppERK1/2 intensity and ERK1/2 N:C ratio derived from 6 separate experiments ±SEM. (**B**, **D**, **F** and **H**) Cell populations pooled from 3 independent experiments were sorted into frequency histograms of ppERK1/2 staining intensity (**B** and **F**) and ERK1/2 N:C ratio (**C** and **G**). (**D** and **H**) Cells were imaged and analysed as described in (A and D) after stimulation for 0, 5, 120 or 360 minutes with 1µM PDBu (as indicated). To compare ppERK1/2 to ERK1/2 N:C ratio, cells were sorted into cell subpopulations of defined (40-80 AFU) ppERK1/2 staining intensity, before calculating the average ERK1/2 N:C value within each subpopulation (or "bin", as described in Fig. 2B). The graphs are plotted as average ppERK1/2 stain intensity within each 40-80 AFU bin against the average N:C ERK ratio for that bin. Data are shown ± SEM of individual cells with each bin containing data from >50 cells.
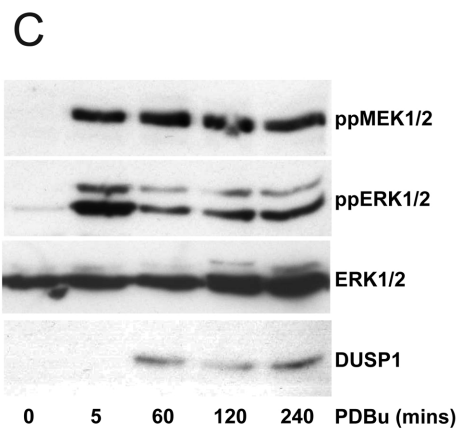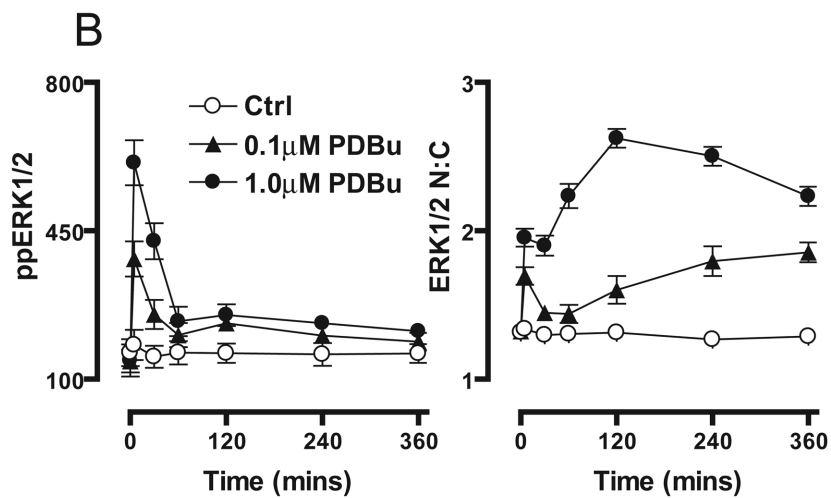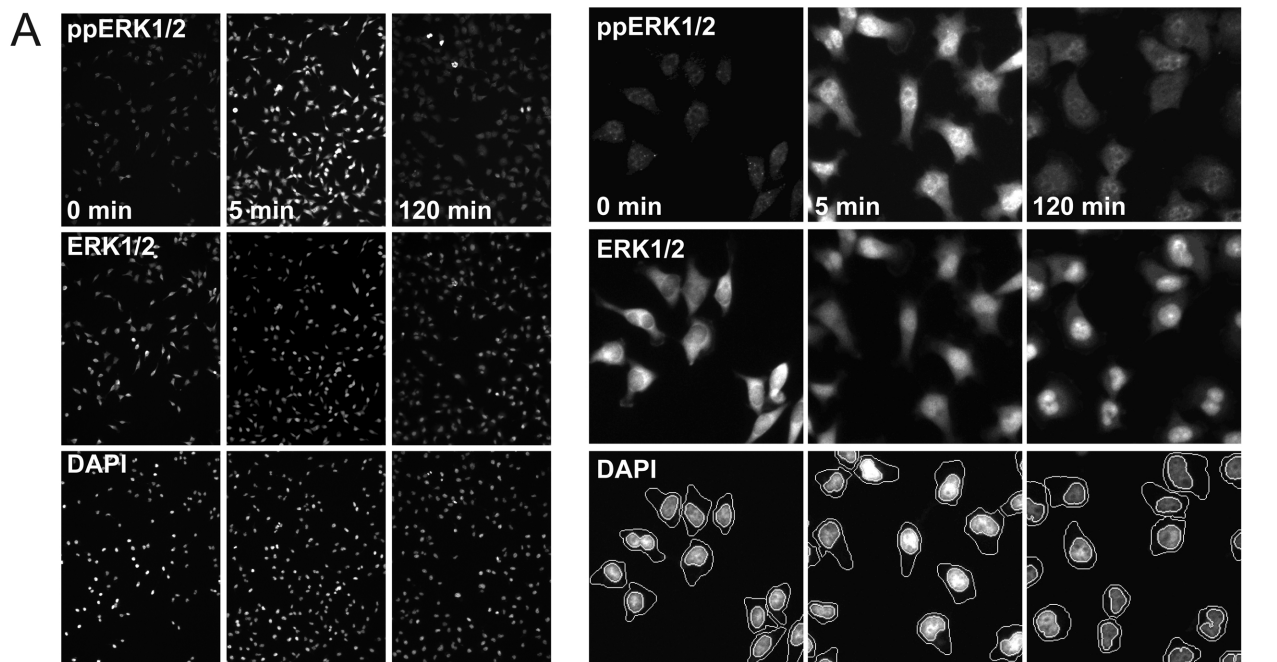
Fig. 1

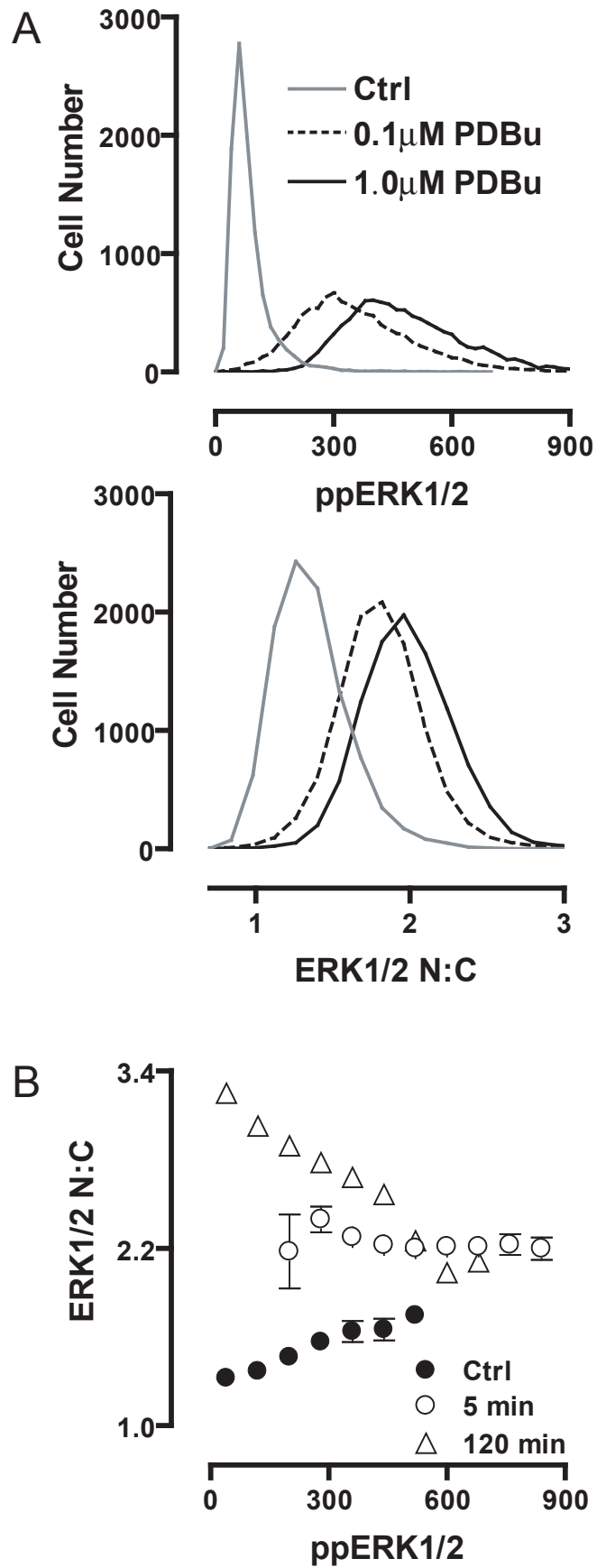A

ppERK1/2	ppERK1/2
ERK1/2	ERK1/2
DAPI	DAPI

0 min   5 min   120 min

B

ppERK1/2

○ Ctrl
▲ 0.1μM PDBu
● 1.0μM PDBu

ERK1/2 N:C

Time (mins)

C

ppMEK1/2
ppERK1/2
ERK1/2
DUSP1

0   5   60   120   240   PDBu (mins)

Fig. 2

Fig. 3

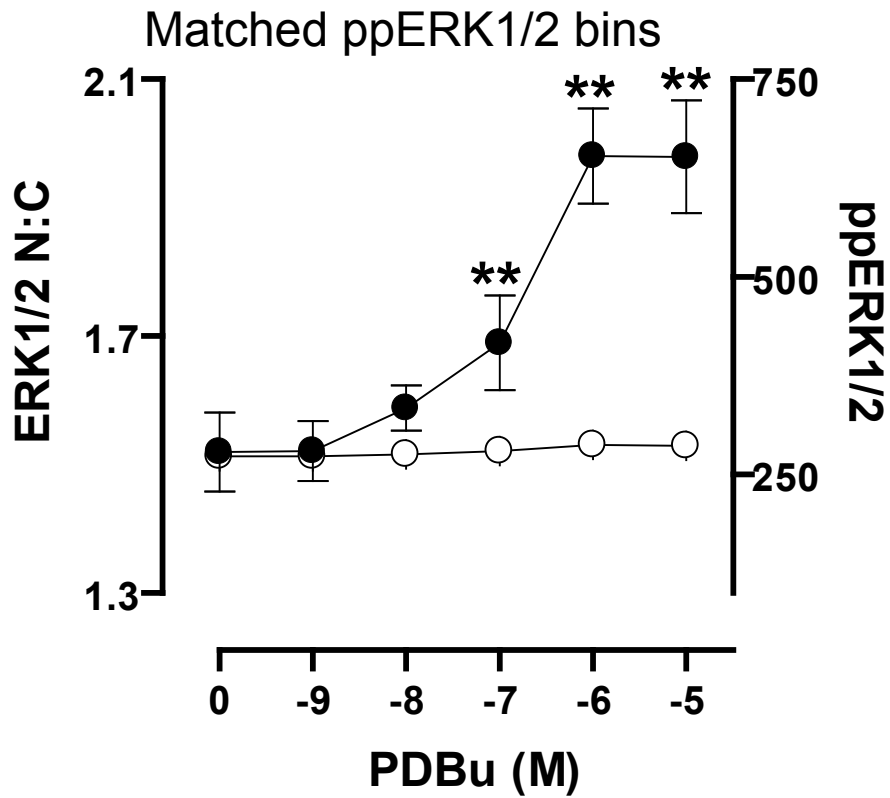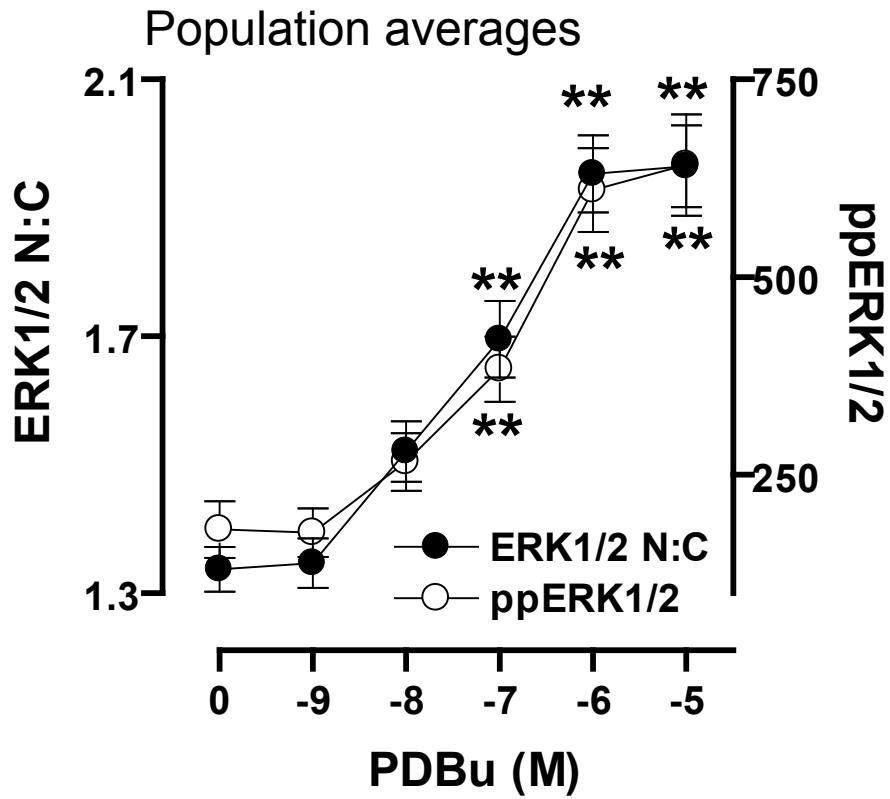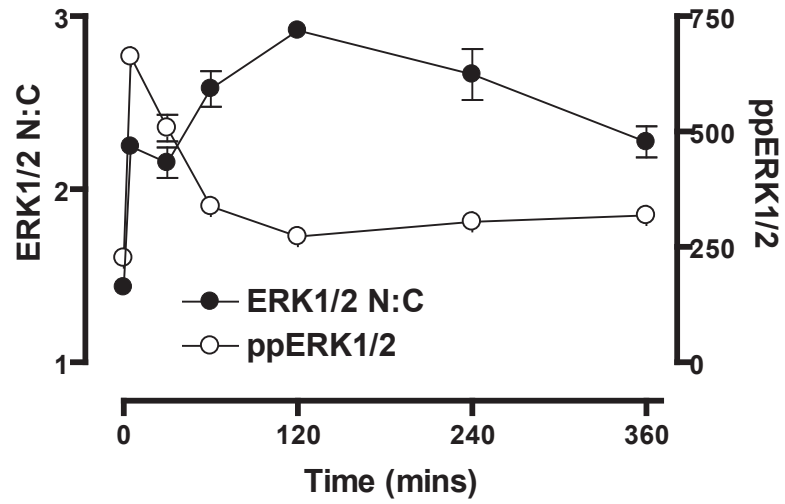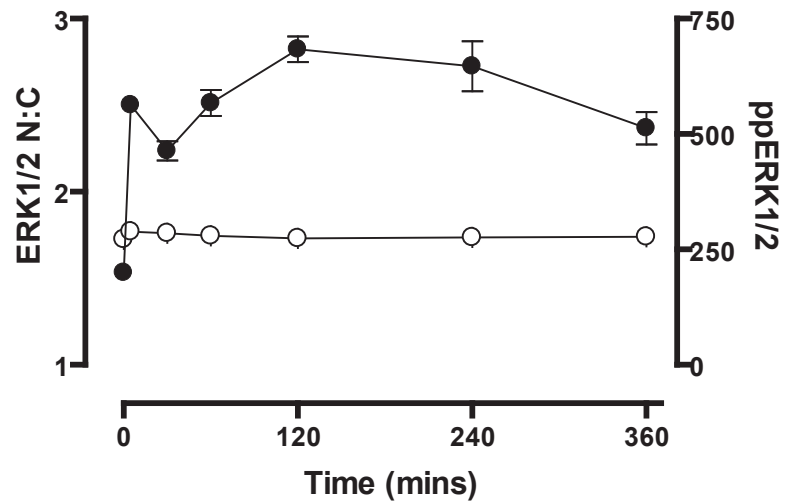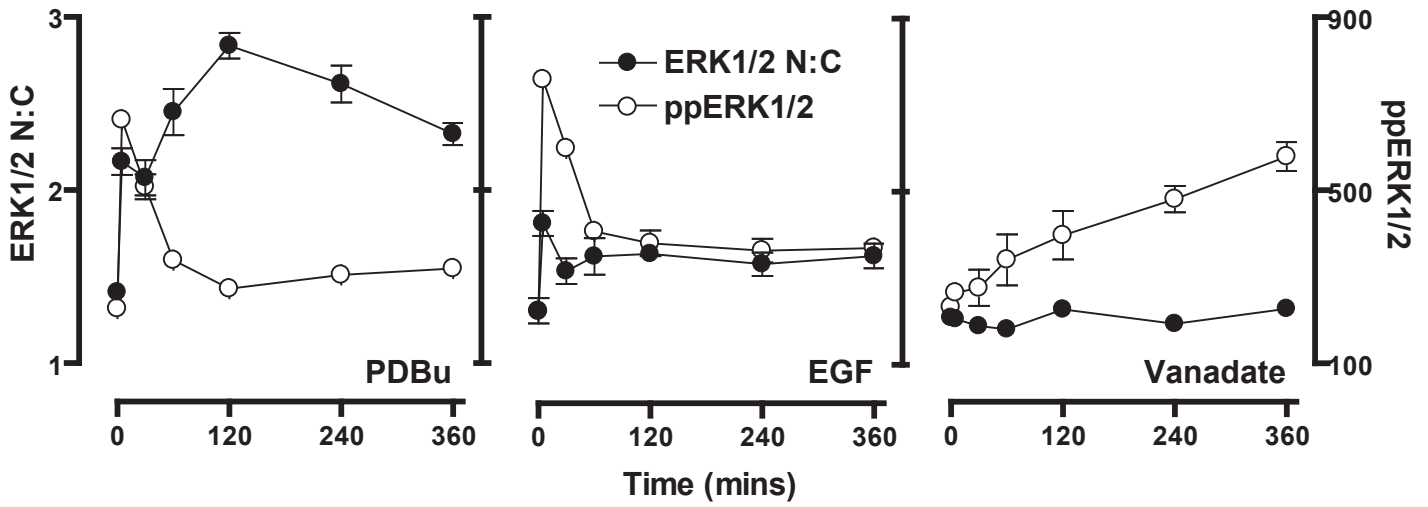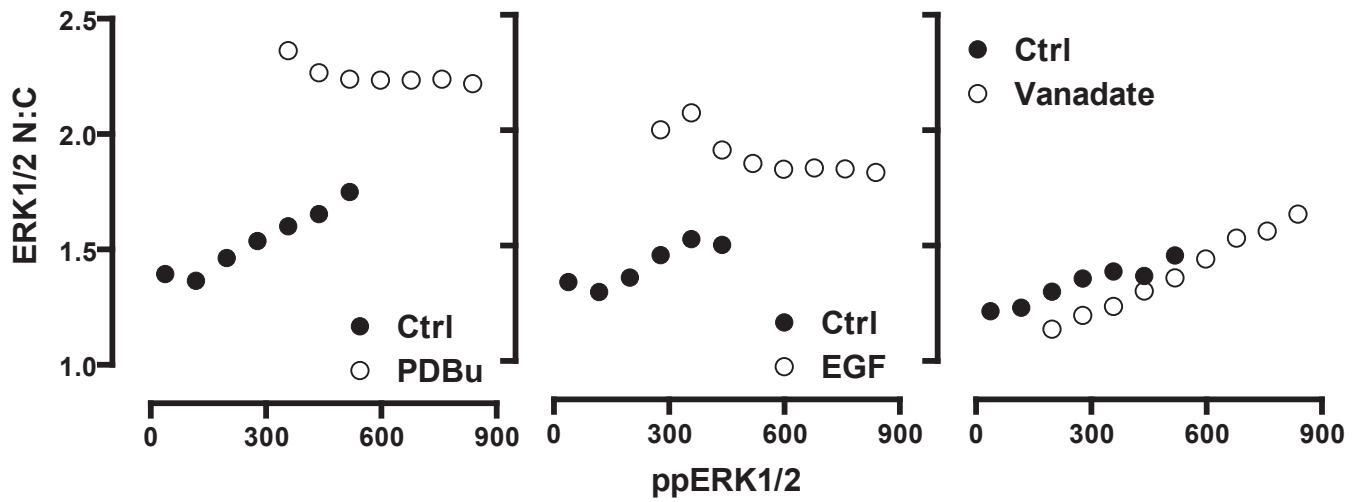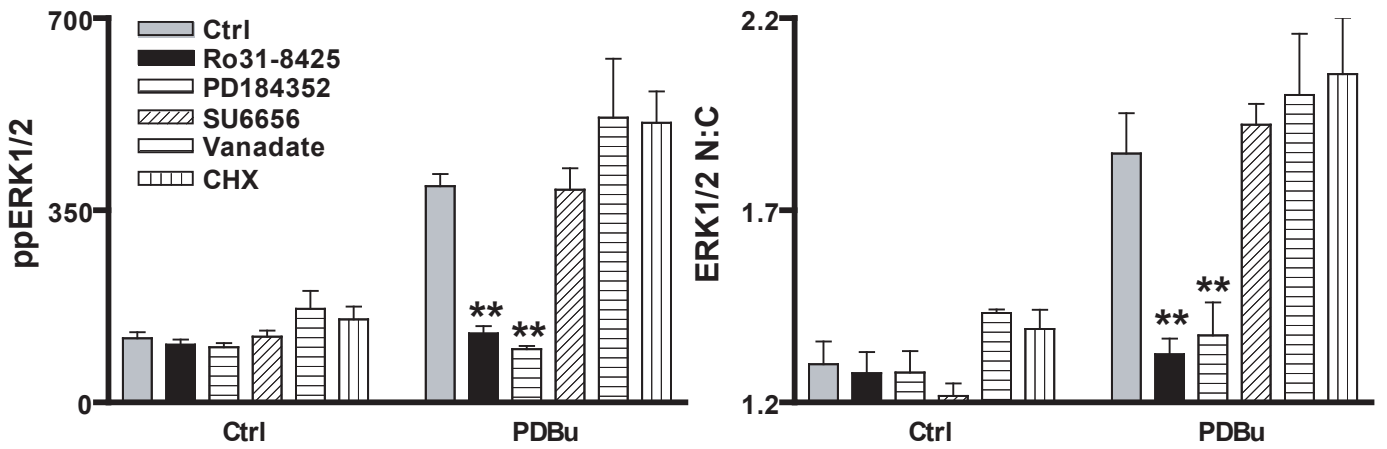Population averages

Matched ppERK1/2 bins

Fig. 4

A Population averages

B Matched ppERK1/2 bins

Fig. 5

A   Population averages

B   Matched ppERK1/2 bins

Fig. 6

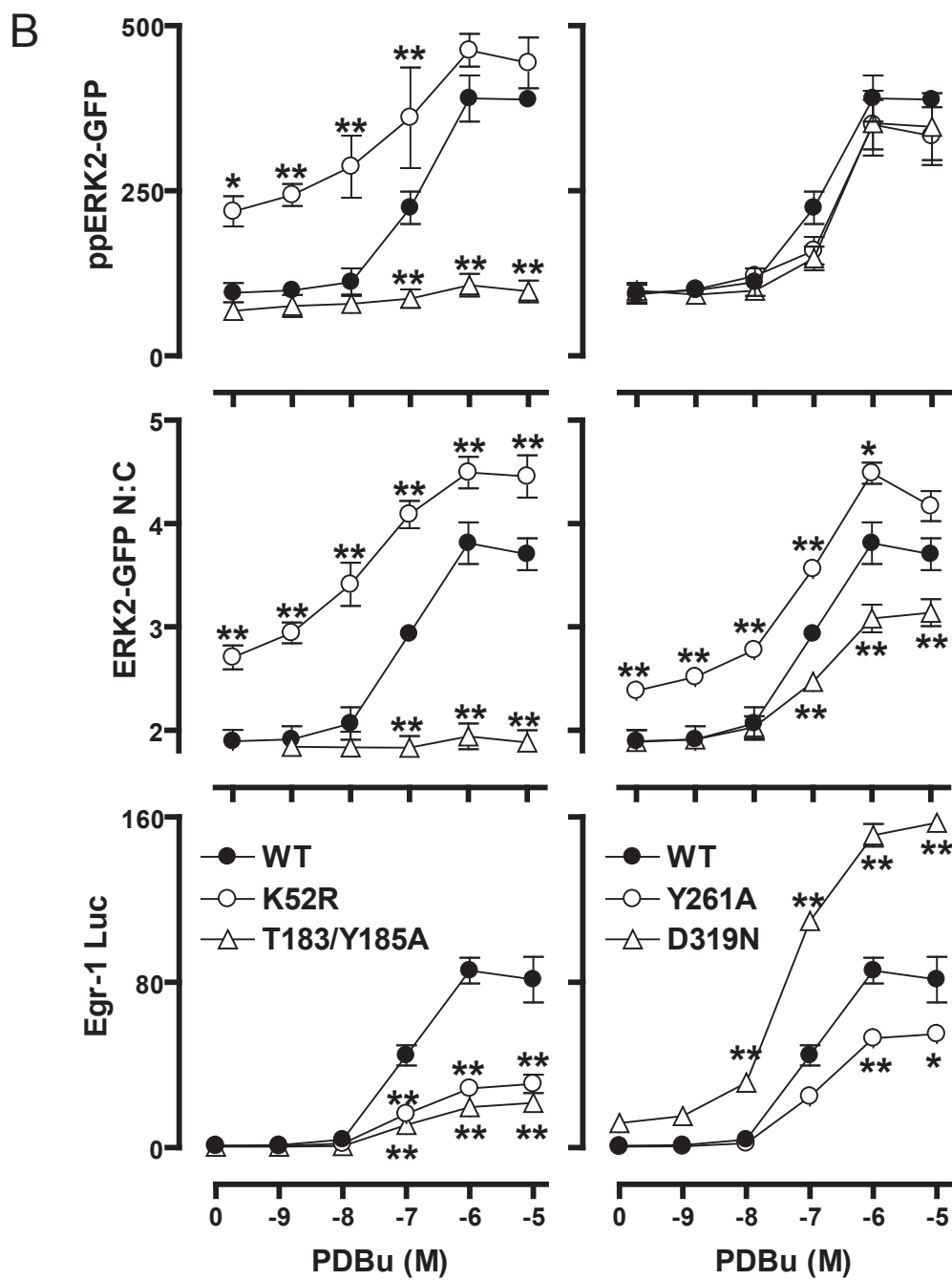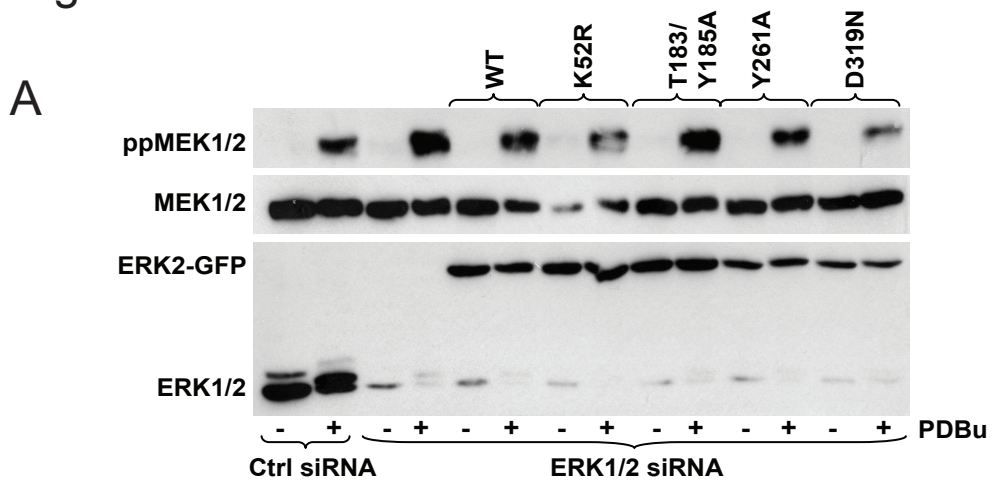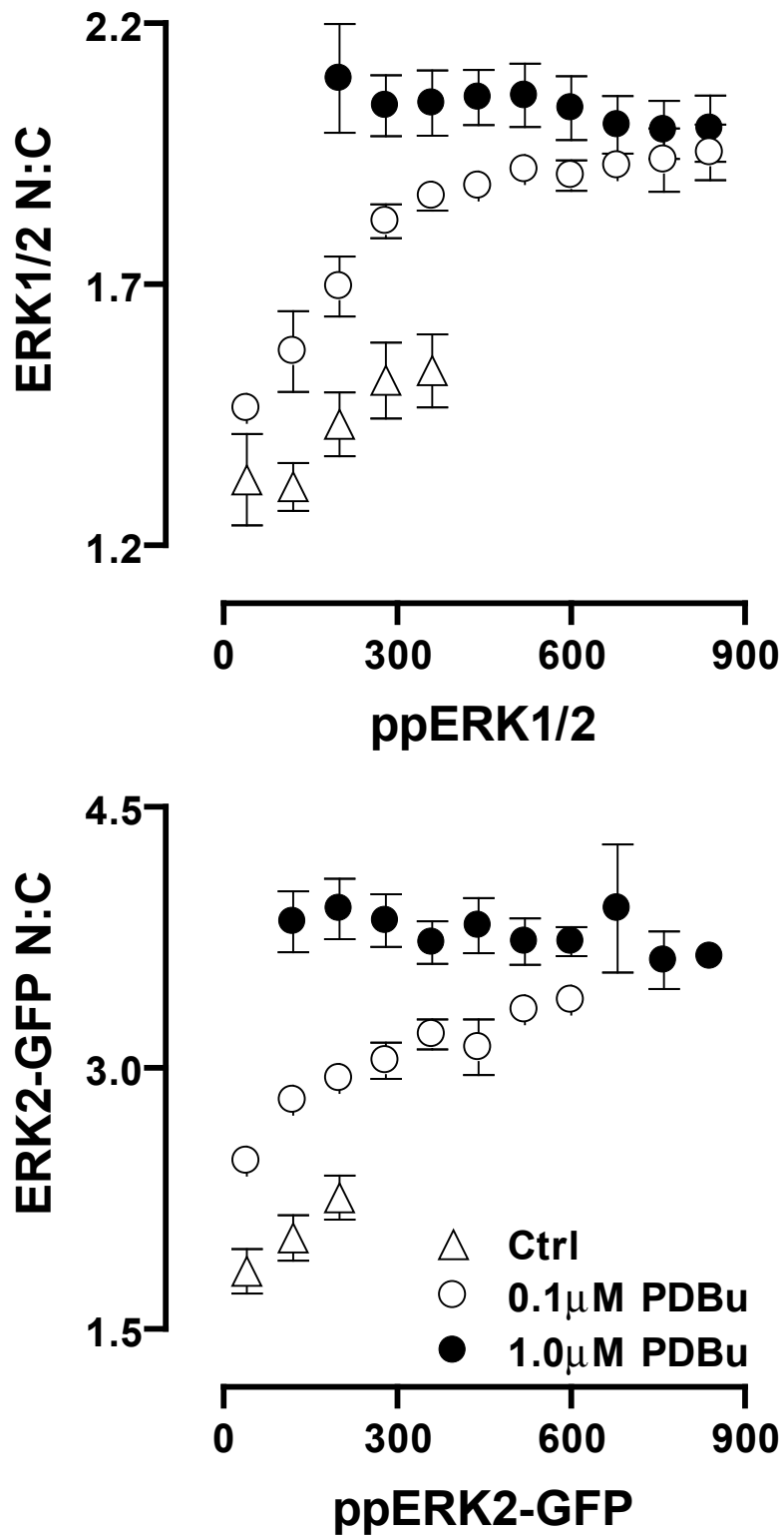A   Population averages

B   Matched ppERK1/2 bins

Fig. 7

Fig. 8

Fig. 9